

Article

Effect of Minor Co Substitution for Fe on the Formability and Magnetic and Magnetocaloric Properties of the Amorphous Fe₈₈Ce₇B₅ Alloy[†]

Xu Zhou¹, Qiang Wang¹ , Leling Pan¹, Ding Ding¹ , Benzen Tang², Peng Yu², Jinlei Yao³ and Lei Xia^{1,*} 

¹ Institute of Materials, Shanghai University, Shanghai 200072, China; zhoxu961228@shu.edu.cn (X.Z.); mat_wq@shu.edu.cn (Q.W.); panleling@shu.edu.cn (L.P.); d.ding@shu.edu.cn (D.D.)

² Chongqing Key Laboratory of Photo-Electric Functional Materials, College of Physics and Electronic Engineering, Chongqing Normal University, Chongqing 401331, China; bz.tang@cqnu.edu.cn (B.T.); pengyu@cqnu.edu.cn (P.Y.)

³ Jiangsu Key Laboratory of Micro and Nano Heat Fluid Flow Technology and Energy Application, School of Physical Science and Technology, Suzhou University of Science and Technology, Suzhou 215009, China; jlyao@usts.edu.cn

* Correspondence: xialei@shu.edu.cn; Tel.: +86-021-6613-5067

[†] Unless otherwise specified all compositions are in atomic percentage in this paper.

Abstract: A small amount of Co was added to the Fe₈₈Ce₇B₅ glass forming alloy for the possibility of improving its glass formability and magnetocaloric effect. The Curie temperature of the amorphous Fe_{88-x}Ce₇B₅Co_x ($x = 0, 1, 2, 3$) ribbons increases linearly with the Co content, while the maximum magnetic entropy change ($-\Delta S_m^{peak}$) increases to 3.89 J/(kg × K) under 5 T at $x = 1$ and subsequently decreases with further Co addition. The mechanism for the influence of Co addition on magnetic properties and the magnetocaloric effect of the amorphous alloys was investigated. Furthermore, a flattened $-\Delta S_m$ profile was designed in the amorphous laminate composed of the amorphous Fe_{88-x}Ce₇B₅Co_x ($x = 0, 1, 2$) ribbons. The high average $-\Delta S_m$ from ~287 K to ~320 K indicates the potential application perspective of the amorphous hybrid as a magnetic refrigerant of a domestic refrigerator.

Keywords: amorphous alloy; glass formability; Curie temperature; magnetic entropy change



Citation: Zhou, X.; Wang, Q.; Pan, L.; Ding, D.; Tang, B.; Yu, P.; Yao, J.; Xia, L. Effect of Minor Co Substitution for Fe on the Formability and Magnetic and Magnetocaloric Properties of the Amorphous Fe₈₈Ce₇B₅ Alloy. *Metals* **2022**, *12*, 589. <https://doi.org/10.3390/met12040589>

Academic Editor: Alexander McLean

Received: 4 March 2022

Accepted: 29 March 2022

Published: 30 March 2022

Publisher's Note: MDPI stays neutral with regard to jurisdictional claims in published maps and institutional affiliations.



Copyright: © 2022 by the authors. Licensee MDPI, Basel, Switzerland. This article is an open access article distributed under the terms and conditions of the Creative Commons Attribution (CC BY) license (<https://creativecommons.org/licenses/by/4.0/>).

1. Introduction

With the increasing shortage of energy and the worsening environmental pollution, it is vitally urgent to develop new refrigeration technology to replace the vapor expansion/compression refrigerators because the traditional refrigeration technology is of low refrigeration efficiency and is not eco-friendly. The magnetic refrigerators based on the magnetocaloric effect (MCE) of magnetic materials are regarded as one of the potential alternatives to the traditional refrigerators because of their energy conservation (at least 30%), eco-friendliness due to their free of ozone-depleting gases, and compactness due to the use of solid refrigerants [1,2].

The MCE refers to the heating of a magnetic material upon magnetization under an adiabatic condition induced by the decrease of magnetic entropy due to the ordering of magnetic moment [3]. Materials exhibiting excellent MCE are considered to be suitable for application as magnetic refrigerants. The magnetic refrigerator generally undergoes an Ericsson cycle, and thus the magnetic refrigerant should better exhibit a table-like magnetic entropy change ($-\Delta S_m$) profile within the working temperature range of a magnetic refrigerator [4]. However, the table-like $-\Delta S_m$ profile can hardly be achieved in a single alloy or compound; instead, it is usually achieved in composites composed of several alloys or compounds with Curie temperatures (T_c) ranging from the cold end (T_{cold}) to the hot end (T_{hot}) of a magnetic refrigerator [5–9]. Obviously, the broad $-\Delta S_m$ hump of the alloys

experiencing 2nd-order magnetic phase transition (MPT) behavior rather than the narrow $-\Delta S_m$ peak of 1st-order MPT alloys, and the tunable Curie temperature of the alloys, are essential for constructing the table-like $-\Delta S_m$ profile.

Amorphous alloys (AAs) can perfectly match the above requirements, not only because they experience a 2nd-order MPT and exhibit a broadened $-\Delta S_m$ hump but also due to their tailorable T_c within a wide temperature range by compositional adjustment [10–22]. The major challenge for the AAs to be used as magnetic refrigerants is how to enhance the $-\Delta S_m$ as much as possible. The rare earth (RE)-based AAs, typically the Gd-based bulk metallic glasses, show outstanding glass formability as well as rather large peak value of magnetic entropy change ($-\Delta S_m^{peak}$) at low temperature [10–12]. However, the RE-based metallic glasses are expensive, and the alloys with T_c near room temperature (RT) usually show poor glass formability and low $-\Delta S_m^{peak}$ [13]. The transition metal (TM)-based metallic glasses with T_c near RT are less expensive and can be easily fabricated, but their $-\Delta S_m$ peak values are very low. For instance, the Fe-Zr-B-based AAs show better MCE in the iron-based metallic glasses near the ambient temperature, but most of their $-\Delta S_m^{peak}$ are not higher than 3.2 J/(kg × K) under 5 T [14–17]. The minor substitution of Co for Fe can obviously improve the $-\Delta S_m^{peak}$ of the Fe-Zr-B amorphous ribbons to above 3.2 J/(kg × K) under 5 T, or even to about 3.4 J/(kg × K) under 5 T at 2% (at.%) Co, but they simultaneously enhance their Curie temperature to above 330 K, which is well higher than RT [18,19].

More recently, we successfully fabricated the Fe-La/Ce-B metallic glasses and achieved better magnetocaloric properties with $-\Delta S_m^{peak}$ of at least 10% larger than those of the Fe-Zr-B-based AAs near the ambient temperature [20,21]. In this paper, we selected a Fe₈₈Ce₇B₅ AA with a $-\Delta S_m^{peak}$ of ~ 3.83 J/(kg × K) under 5 T at 287 K [22] as a basic alloy and prepared the Fe_{88-x}Ce₇B₅Co_x ($x = 1, 2, 3$) amorphous ribbons. The effect of minor Co replacement for Fe on the glass formability, magnetic properties and MCE of the ternary amorphous alloy, as well as the mechanisms involved, was studied.

2. Materials and Methods

The master ingots with nominal Fe_{88-x}Ce₇B₅Co_x ($x = 1, 2, 3$) compositions were prepared one by one by arc-melting the mixture of raw materials several times using a non-consumable electrode in a high vacuum furnace (PhyScience Opto-electronics, Beijing, China) filled with high-purity Ar. The ingots were manufactured to be the shape of ~40-μm-thickness ribbons under a high-purity Ar atmosphere by a melt-spinning method at a wheel surface speed of 50 m/s. The amorphous features of the as-spun Fe_{88-x}Ce₇B₅Co_x ($x = 1, 2, 3$) ribbons were ascertained by their X-ray diffraction (XRD) patterns measured by a Rigaku D\max-rC diffractometer (Rigaku, Tokyo, Japan) with Cu K_α radiation [23]. The glass formability of the amorphous ribbons was evaluated from the thermal properties obtained from their differential scanning calorimetry (DSC) traces measured by a NET-ZSCH 404C calorimeter (Netzsch, Selb, Germany) [24] at a heating rate of 20 K/min. The temperature and field dependence of magnetization curves were measured by a vibrating sample magnetometer (VSM), which is a module of a Physical Property Measurement System (PPMS, model 6000, Quantum Design, San Diego, CA, USA) [25]. The Arrott plots were derived from the isothermal magnetization (M - H) curves to confirm the type of phase transition. The $-\Delta S_m$ vs. temperature curves were constructed from M - H curves according to the Maxwell equation. The $-\Delta S_m$ of the amorphous hybrid was calculated as

$$-\Delta S_m(\text{hybrid}) = \sum_{i=1, 2, \dots, n}^n w_i \times (-\Delta S_m)_i \quad (1)$$

where w_i is the weight fraction of an amorphous ribbon.

3. Results and Discussion

The X-ray diffraction results of the as-spun $\text{Fe}_{88-x}\text{Ce}_7\text{B}_5\text{Co}_x$ ($x = 1, 2, 3$) ribbons are displayed in Figure 1a. The ribbons show smooth and broad diffraction humps, indicating that all the as-spun $\text{Fe}_{88-x}\text{Ce}_7\text{B}_5\text{Co}_x$ ($x = 1, 2, 3$) ribbons are amorphous. From the DSC traces of the three samples, as shown in Figure 1b, the endothermic glass transition hump and the exothermic crystallization peaks also ascertain the amorphous characteristics of these samples. Simultaneously, the onset temperatures of glass transition (T_g) and primary crystallization (T_x), as well as the liquid temperature (T_l) of the $\text{Fe}_{88-x}\text{Ce}_7\text{B}_5\text{Co}_x$ ($x = 1, 2, 3$) ribbons, are listed in Table 1. Therefore, two commonly used criteria for evaluating the glass formability of amorphous alloys, namely, the reduced glass transition temperature (T_{rg} , defined as the ratio of T_g and T_l) [26] and the parameter γ (defined as the ratio of T_x and $(T_g + T_l)$) [27], can be calculated accordingly to be 0.421 and 0.368 for $\text{Fe}_{87}\text{Ce}_7\text{B}_5\text{Co}_1$, 0.426 and 0.361 for $\text{Fe}_{86}\text{Ce}_7\text{B}_5\text{Co}_2$, 0.437 and 0.360 for $\text{Fe}_{85}\text{Ce}_7\text{B}_5\text{Co}_3$. Compared to the $\text{Fe}_{88}\text{Ce}_7\text{B}_5$ ribbon, the minor Co substitution for Fe dramatically decreases the T_g , which decreases the T_{rg} and reaches a minimum at $x = 1$ but obviously enlarges the supercooled liquid region ($\Delta T_x = T_x - T_g$ [28], also listed in Table 1), which makes the γ value reach to a maximum at $x = 1$, as illustrated in Figure 1c. Overall, both the T_{rg} and γ of the $\text{Fe}_{88-x}\text{Ce}_7\text{B}_5\text{Co}_x$ ($x = 0, 1, 2, 3$) ribbons are in accordance with their glass formability: they can be quenched into amorphous ribbons easily but are not able to be vitrified into bulk amorphous samples.

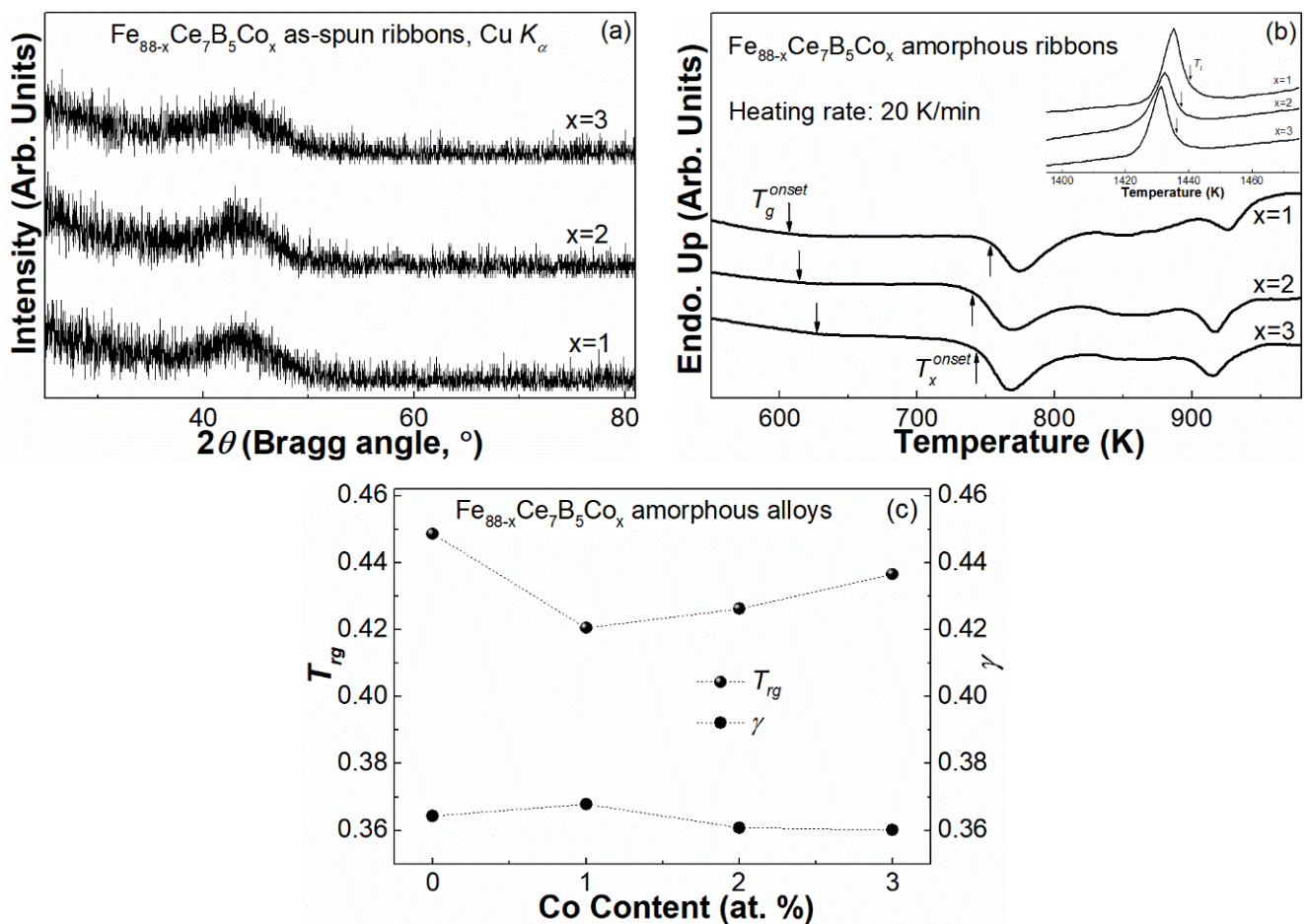


Figure 1. (a) XRD patterns and (b) DSC curves of the $\text{Fe}_{88-x}\text{Ce}_7\text{B}_5\text{Co}_x$ ($x = 1, 2, 3$) as-spun ribbons; the inset is the melting behaviors. (c) The compositional dependence of T_{rg} and γ for these amorphous ribbons.

Table 1. The thermal properties of the $\text{Fe}_{88-x}\text{Ce}_7\text{B}_5\text{Co}_x$ ($x = 0, 1, 2, 3$) amorphous ribbons.

$\text{Fe}_{88-x}\text{Ce}_7\text{B}_5\text{Co}_x$	T_g (K)	T_x (K)	T_l (K)	ΔT_x (K)	T_{rg}	γ
$x = 0$	647	761	1442	114	0.449	0.364
$x = 1$	606	753	1441	147	0.421	0.368
$x = 2$	613	740	1438	127	0.426	0.361
$x = 3$	627	743	1436	116	0.437	0.360

Figure 2a shows the hysteresis loops under 5 Tesla of the $\text{Fe}_{88-x}\text{Ce}_7\text{B}_5\text{Co}_x$ ($x = 1, 2, 3$) glassy samples measured at 180 K and 380 K, respectively. All these samples show soft magnetic at 180 K and almost paramagnetic at 380 K, indicating that the ferromagnetic-paramagnetic transition occurs within 180 K and 380 K. The saturation magnetization is approximately $144.4 \text{ Am}^2/\text{kg}$ for $x = 1$, $145.0 \text{ Am}^2/\text{kg}$ for $x = 2$ and $144.0 \text{ Am}^2/\text{kg}$ for $x = 3$, which implies the slightly fluctuation of the magnetic moment with the Co addition. The temperature dependence of magnetization curves for the $\text{Fe}_{88-x}\text{Ce}_7\text{B}_5\text{Co}_x$ ($x = 1, 2, 3$) ribbons was measured under 300 Oe after a zero-field-cooling operation, as shown in Figure 2b. The T_c , which is obtained at the minimum of dM/dT , can be found to be 305 K for $\text{Fe}_{87}\text{Ce}_7\text{B}_5\text{Co}_1$, 323 K for $\text{Fe}_{86}\text{Ce}_7\text{B}_5\text{Co}_2$, and 346 K for $\text{Fe}_{85}\text{Ce}_7\text{B}_5\text{Co}_3$. Similar to the situation in the Co substituted $\text{Fe}_{88}\text{Zr}_8\text{B}_4$ amorphous ribbons [19], T_c of the $\text{Fe}_{88-x}\text{Ce}_7\text{B}_5\text{Co}_x$ ($x = 0, 1, 2, 3$) amorphous ribbons increases linearly with the Co content, as shown in the inset of Figure 2b, which is attributed to the enhanced $3d$ - $3d$ interaction between $3d$ atoms by the Co addition [29]. As shown in Figure 3a for $x = 1$, Figure 3b for $x = 2$, and Figure 3c for $x = 3$, the magnetic phase transition of the $\text{Fe}_{88-x}\text{Ce}_7\text{B}_5\text{Co}_x$ ($x = 1, 2, 3$) amorphous samples was confirmed to be 2nd-order MPT by the Arrott plots at various temperatures derived from their isothermal magnetization (M - H) curves (illustrated in the inset of Figure 3a–c, respectively).

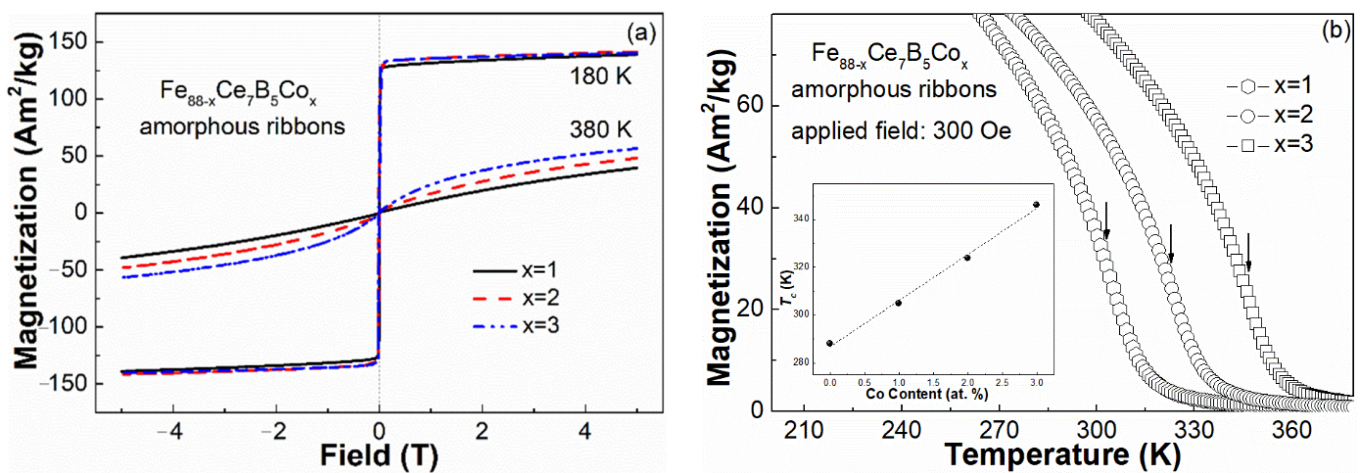


Figure 2. (a) The hysteresis loops of the $\text{Fe}_{88-x}\text{Ce}_7\text{B}_5\text{Co}_x$ ($x = 1, 2, 3$) amorphous ribbons measured at 180 and 380 K under 5 T. (b) M - T curves of these amorphous ribbons under 300 Oe; the inset is the relationship between T_c and Co content.

The magnetic phase transition from ferromagnetic to paramagnetic usually results in the reduction of magnetic entropy due to the ordering of magnetic moments. Figure 4 illustrates the relationship between $-\Delta S_m$ and temperature ($(-\Delta S_m)$ - T curve) under various fields of the $\text{Fe}_{88-x}\text{Ce}_7\text{B}_5\text{Co}_x$ (a) for $x = 1$, (b) for $x = 2$, and (c) for $x = 3$) amorphous ribbons. The three AAs show typical broad $-\Delta S_m$ hump of 2nd-order MPT materials, and the $-\Delta S_m^{peak}$ were observed near T_c on each $(-\Delta S_m)$ - T curve. The $-\Delta S_m^{peak}$ under different fields of the ribbons are summarized in Table 2, accompanied with that of the $\text{Fe}_{88}\text{Ce}_7\text{B}_5$ amorphous ribbon for comparison purposes. It was found that $-\Delta S_m^{peak}$ of $\text{Fe}_{88}\text{Ce}_7\text{B}_5$ AA was improved by adding 1% (at. %) Co but was decreased by adding more Co. As the

average magnetic moment of Co atoms is lower than that of the Fe atoms, the $-\Delta S_m^{peak}$ of the $Fe_{88-x}Ce_7B_5Co_x$ ($x = 0, 1, 2, 3$) AAs should be generally decreased with the Co addition. The slightly increased $-\Delta S_m^{peak}$ at $x = 1$ may be induced by the extra $3d-3d$ interaction between Co and Fe atoms [30].

According to the Arrott–Noakes equation, the relationship between the $-\Delta S_m$ and the external magnetic fields (H) in an amorphous alloy undergoing a 2nd-order magnetic transition can be expressed as $-\Delta S_m = A \times H^n$, where A is a constant [31]. Figure 4d shows exponent n vs temperature curves of the $Fe_{88-x}Ce_7B_5Co_x$ ($x = 1, 2, 3$) glassy ribbons by linearly fitting $\ln(-\Delta S_m)-\ln(H)$ plots at various temperatures. As predicted by V. Franco [31], n exponent of all the three samples is about 1 at low temperatures well below T_c , subsequently decreases to a minimum (about 0.75) near T_c , and finally approaches to a value of 2 at temperatures much higher than T_c . The values of n near T_c of these three samples, seen in the inset of Figure 4d, are 0.763 for $x = 1$ at 305 K, 0.758 for $x = 2$ at 322.5 K, and 0.756 for $x = 3$ at 347.5 K, all of which agree well with the results of other alloys undergoing a 2nd-order MPT [11,15–21] and indicate the typical magnetocaloric effect of these AAs.

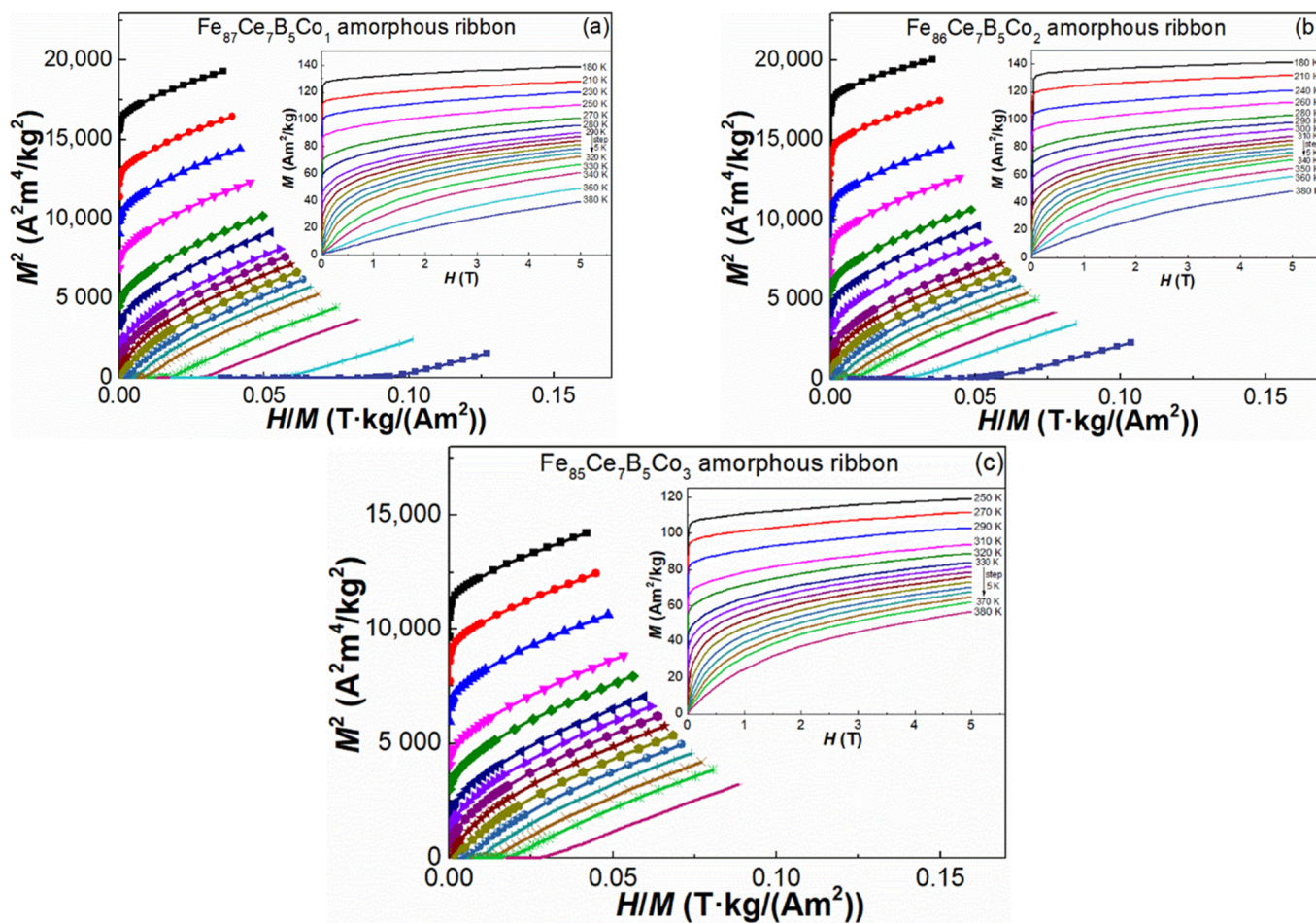


Figure 3. The Arrott plots of the $Fe_{88-x}Ce_7B_5Co_x$ amorphous ribbons: (a) $x = 1$, (b) $x = 2$, and (c) $x = 3$, the insets are the isothermal magnetization curves of these ribbons under 5 T.

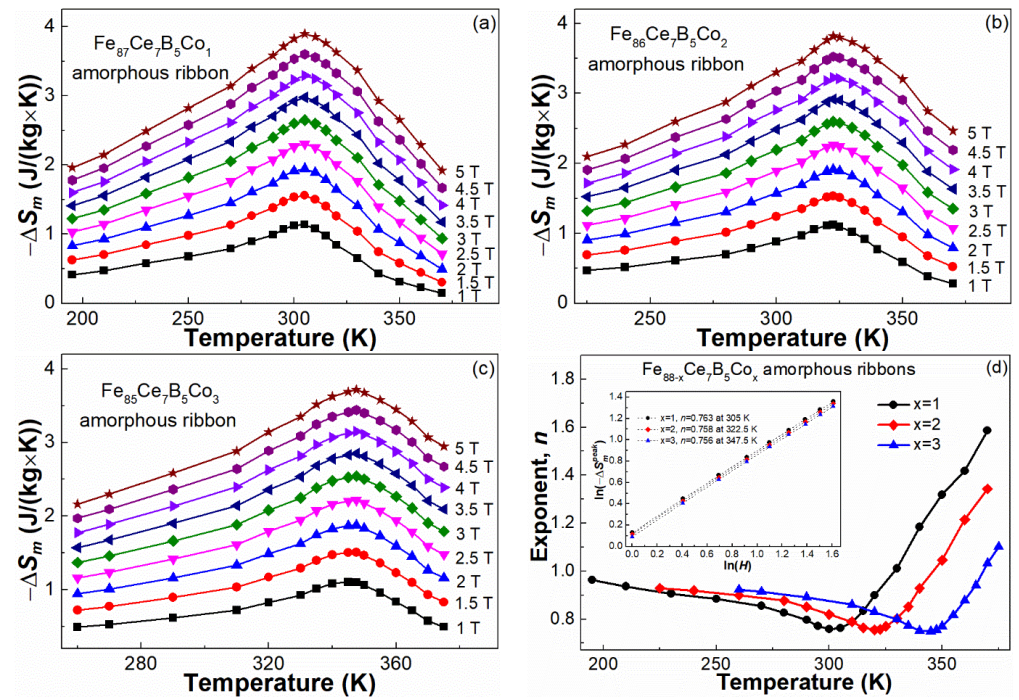


Figure 4. $(-\Delta S_m)$ - T curves of the $\text{Fe}_{88-x}\text{Ce}_7\text{B}_5\text{Co}_x$ amorphous ribbons under various magnetic fields: (a) $x = 1$, (b) $x = 2$, (c) $x = 3$, and (d) n - T curves of the $\text{Fe}_{88-x}\text{Ce}_7\text{B}_5\text{Co}_x$ amorphous ribbons; the inset is the $\ln(-\Delta S_m^{\text{peak}})$ - $\ln(H)$ plots of these ribbons at T_c .

Table 2. $-\Delta S_m^{\text{peak}}$ and T_c of some Fe-based amorphous alloys near room temperature.

Composition	$-\Delta S_m^{\text{peak}}$ (J/(kg × K))					T_c (K)	Ref.
	1 T	1.5 T	2 T	3 T	5 T		
$\text{Fe}_{88}\text{Ce}_7\text{B}_5$	1.12	1.54	1.91	2.60	3.83	287	[22]
$\text{Fe}_{87}\text{Ce}_7\text{B}_5\text{Co}_1$	1.15	1.56	1.95	2.65	3.89	305	This work
$\text{Fe}_{86}\text{Ce}_7\text{B}_5\text{Co}_2$	1.13	1.54	1.91	2.60	3.82	323	
$\text{Fe}_{85}\text{Ce}_7\text{B}_5\text{Co}_3$	1.10	1.51	1.88	2.54	3.72	346	
$\text{Fe}_{83}\text{Nd}_5\text{Cr}_8\text{B}_4$	-	-	1.8	-	3.4	322	[9]
$\text{Fe}_{80}\text{Nd}_8\text{Cr}_8\text{B}_4$	-	-	1.8	-	3.5	340	
$\text{Fe}_{80}\text{B}_{10}\text{Zr}_9\text{Cu}_1$	1.04	-	1.72	-	3.28	356	[14]
$\text{Fe}_{77}\text{Ta}_3\text{B}_{10}\text{Zr}_9\text{Cu}_1$	0.93	-	1.47	-	2.84	336	
$\text{Fe}_{75}\text{Ta}_5\text{B}_{10}\text{Zr}_9\text{Cu}_1$	0.68	-	1.04	-	2.03	313	
$\text{Fe}_{88}\text{Zr}_9\text{B}_3$	0.94	1.28	1.59	2.16	3.17	286	[15]
$\text{Fe}_{87}\text{Zr}_9\text{B}_4$	0.99	1.35	1.67	2.26	3.29	304	
$\text{Fe}_{86}\text{Zr}_9\text{B}_5$	1.02	1.39	1.72	2.3	3.34	327	
$\text{Fe}_{88}\text{Zr}_8\text{B}_4$	0.88	1.20	1.50	2.06	3.04	291	[16]
$\text{Fe}_{87}\text{Zr}_8\text{B}_5$	0.94	1.29	1.61	2.19	3.25	306	
$\text{Fe}_{87}\text{Zr}_7\text{B}_4\text{Co}_2$	1.01	1.38	1.72	2.34	3.42	333	[18]
$\text{Fe}_{87}\text{Co}_1\text{Zr}_8\text{B}_4$	0.93	1.29	1.61	2.2	3.24	317	[19]
$\text{Fe}_{86}\text{Co}_2\text{Zr}_8\text{B}_4$	0.98	1.35	1.69	2.31	3.38	340	
$\text{Fe}_{86}\text{La}_7\text{Ce}_2\text{B}_5$	-	1.45	-	-	3.64	313	[20]
$\text{Fe}_{82}\text{Ce}_{12}\text{B}_6$	-	-	1.78	-	3.54	284	[32]
$\text{Fe}_{82.5}\text{Ce}_{11.5}\text{B}_6$	-	-	1.91	-	3.81	291	
$\text{Fe}_{83}\text{Ce}_{11}\text{B}_6$	-	-	1.96	-	3.90	297	
$\text{Fe}_{85}\text{Co}_3\text{Zr}_5\text{B}_4\text{Nb}_3$	1.03	1.41	1.76	2.41	3.55	336	[33]
$\text{Fe}_{87}\text{Zr}_8\text{B}_4\text{Sm}_1$	0.98	1.33	1.65	2.24	3.27	308	[34]
$\text{Fe}_{86}\text{Zr}_8\text{B}_4\text{Sm}_2$	1.04	1.41	1.73	2.32	3.35	325	
$\text{Fe}_{85}\text{Zr}_8\text{B}_4\text{Sm}_3$	1.09	1.47	1.81	2.44	3.55	333	
$\text{Fe}_{86}\text{Zr}_8\text{B}_4\text{Mn}_2$	0.87	-	1.47	2.00	2.93	283	[35]
$\text{Fe}_{66.3}\text{B}_{12}\text{Si}_8\text{V}_{13.7}$	-	-	-	-	1.8	334	[36]
$\text{Fe}_{79}\text{Gd}_1\text{Cr}_8\text{B}_{12}$	1.12	1.42	-	-	3.59	355	[37]

Figure 5a shows the $-\Delta S_m^{peak}$ under 5 T of various iron-based metallic glasses with T_c ranging from 280 K to 360 K (also listed in Table 2). The $-\Delta S_m^{peak}$ of the Fe(Co)-Ce-B glassy alloys are comparable to or even larger than those of most iron-based metallic glasses around RT [9,14–16,18–20,32–37]. For example, the $-\Delta S_m^{peak}$ of the $Fe_{87}Ce_7B_5Co_1$ amorphous ribbon (3.89 J/(kg × K) under 5 T) is comparable to that of the $Fe_{83}Ce_{11}B_6$ glassy alloy [32], which is the largest among those metallic glasses. The $-\Delta S_m^{peak}$ of the $Fe_{85}Ce_7B_5Co_3$ amorphous ribbon, which is the lowest $-\Delta S_m^{peak}$ value among the $Fe_{88-x}Ce_7B_5Co_x$ ribbons, is still higher than the $-\Delta S_m^{peak}$ of most of those iron-based metallic glasses. On the other hand, it should be noted that the T_c of $Fe_{88}Ce_7B_5$ (287 K) and $Fe_{86}Ce_7B_5Co_2$ (323 K) glassy alloys are close to the T_{cold} and T_{hot} of a domestic air conditioner. Therefore, high $-\Delta S_m^{peak}$ of the $Fe_{88-x}Ce_7B_5Co_x$ metallic glasses allows us to construct a specific table-like $-\Delta S_m$ profile within temperature interval from 280 K to 320 K in an amorphous hybrid composed of these amorphous ribbons. Figure 5b displays the table-like $(-\Delta S_m)-T$ curves under 1.5 T and 5 T for an amorphous laminate composed of 49% (wt.%) $Fe_{88}Ce_7B_5$ + 2% (wt.%) $Fe_{87}Ce_7B_5Co_1$ + 49% (wt.%) $Fe_{86}Ce_7B_5Co_2$ glassy ribbons. The average $-\Delta S_m$ value ($-\Delta S_m^{average}$) of the amorphous laminate is about 1.28 J/(kg × K) under 1.5 T from 280 K to 315 K, and approximately 3.48 J/(kg × K) under 5 T from 287 K to 320 K; these values are much higher than those of other Fe-Zr-B-based amorphous hybrids [19,34]. Furthermore, the compositions of the amorphous laminate do not contain any radioactive elements and will not bring about some health hazards. Therefore, the high $-\Delta S_m^{average}$ from the T_{cold} to the T_{hot} of the amorphous composite indicates the potential application perspective as magnetic refrigerant in a domestic air conditioner.

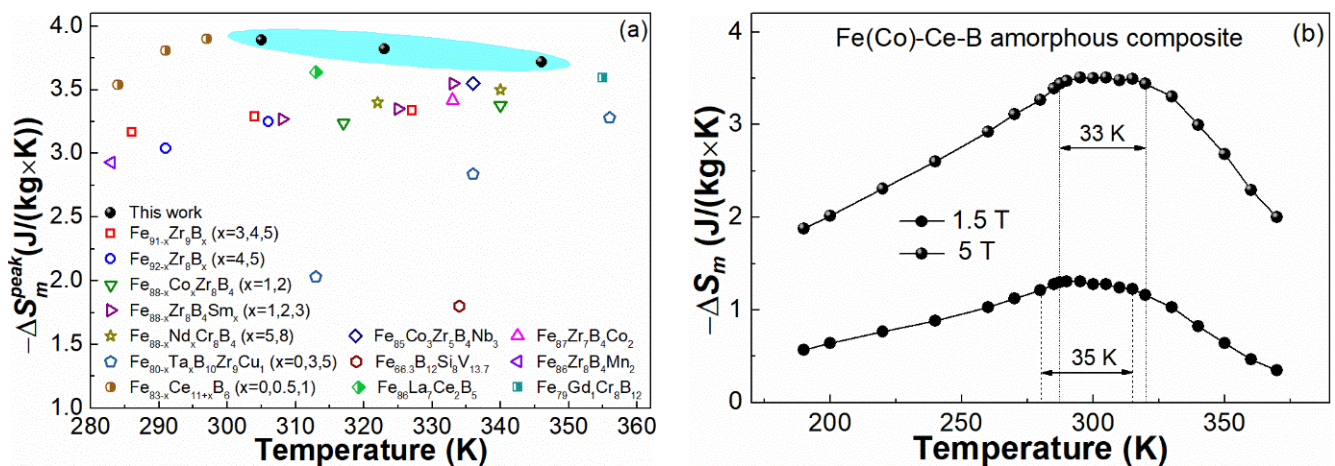


Figure 5. (a) $-\Delta S_m^{peak}$ of various Fe-based metallic glasses with T_c ranging from 280 K to 360 K under 5 T; (b) table-like $(-\Delta S_m)-T$ plots of the amorphous composite composed of Fe(Co)-Ce-B amorphous ribbons under 1.5 T and 5 T.

4. Conclusions

In this work, the $Fe_{88-x}Ce_7B_5Co_x$ ($x = 1, 2, 3$) alloys were successfully fabricated to be about 40- μ m-thickness amorphous ribbons, and the magnetic properties, as well as MCE of these glassy samples, were investigated. All the samples are soft magnetic at 180 K and paramagnetic at 380 K. The T_c of the $Fe_{88-x}Ce_7B_5Co_x$ amorphous ribbons increases linearly from 287 K when $x = 0$ to 305 K when $x = 1$, 323 K when $x = 2$, and 346 K when $x = 3$, which is probably due to the enhanced $3d-3d$ interaction by the Co addition. The Arrott plots as well as the $-\Delta S_m = A \times H^n$ relationship of the amorphous $Fe_{88-x}Ce_7B_5Co_x$ ribbons confirm the typical magnetocaloric behaviors of 2nd-order MPT alloys. The $-\Delta S_m^{peak}$ of these amorphous samples increases to 3.89 J/(kg × K) at $x = 1$ and subsequently decreases with further Co addition, which may be attributed to the compromise of two factors: the decreasing $-\Delta S_m^{peak}$ with Co addition due to the lower average magnetic moment of Co, and the slightly enhanced $-\Delta S_m^{peak}$ due to the introduction of extra $3d-3d$ interaction

between Co and Fe atoms by Co substitution. Based on these results, an amorphous laminate with a table-like $-\Delta S_m$ profile from ~ 280 K to ~ 320 K was achieved by mixing 49% (wt.%) $\text{Fe}_{88}\text{Ce}_7\text{B}_5$ + 2% (wt.%) $\text{Fe}_{87}\text{Ce}_7\text{B}_5\text{Co}_1$ + 49% (wt.%) $\text{Fe}_{86}\text{Ce}_7\text{B}_5\text{Co}_2$ amorphous ribbons. The high $-\Delta S_m^{\text{average}}$ of the amorphous hybrid makes it a better candidate for application as a magnetic refrigerant in a domestic air conditioner.

Author Contributions: Conceptualization, L.X., P.Y. and J.Y.; methodology, D.D.; investigation, X.Z., Q.W. and L.P.; data curation, Q.W. and B.T.; writing—original draft preparation, X.Z., Q.W. and B.T.; writing—review and editing, L.X.; funding acquisition, L.X. and P.Y. All authors have read and agreed to the published version of the manuscript.

Funding: This research was funded by the National Natural Science Foundation of China, grant number 51871139, 52071196 and 52071043.

Institutional Review Board Statement: Not applicable.

Informed Consent Statement: Not applicable.

Data Availability Statement: Data sharing is not applicable.

Acknowledgments: This research was technically supported by the Center for Advanced Microanalysis of Shanghai University.

Conflicts of Interest: The authors declare that they have no conflict of interest to this work.

References

- Gschneidner, K.A., Jr.; Pecharsky, V.K. Rare earths and magnetic refrigeration. *J. Rare Earths* **2006**, *24*, 641–647. [[CrossRef](#)]
- Franco, V.; Blázquez, J.S.; Ipus, J.J.; Law, J.Y.; Moreno-Ramírez, L.M.; Conde, A. Magnetocaloric effect: From materials research to refrigeration devices. *Prog. Mater. Sci.* **2018**, *93*, 112–232. [[CrossRef](#)]
- de Oliveira, N.A.; von Ranke, P.J. Theoretical aspects of the magnetocaloric effect. *Phys. Rep.* **2010**, *489*, 89–159. [[CrossRef](#)]
- Hashimoto, T.; Kuzuhara, T.; Sahashi, M.; Inomata, K.; Tomokiyo, A.; Yayama, H. New application of complex magnetic materials to the magnetic refrigerant in an Ericsson magnetic refrigerator. *J. Appl. Phys.* **1987**, *62*, 3873–3878. [[CrossRef](#)]
- Ma, L.Y.; Gan, L.H.; Chan, K.C.; Ding, D.; Xia, L. Achieving a table-like magnetic entropy change across the ice point of water with tailorable temperature range in Gd-Co-based amorphous hybrids. *J. Alloys Compd.* **2017**, *723*, 197–200. [[CrossRef](#)]
- Álvarez, P.; Sánchez Llamazares, J.L.; Gorria, P.; Blanco, J.A. Enhanced refrigerant capacity and magnetic entropy flattening using a two-amorphous FeZrB(Cu) composite. *Appl. Phys. Lett.* **2011**, *99*, 232501. [[CrossRef](#)]
- Feng, J.Q.; Liu, Y.H.; Sui, J.H.; He, A.N.; Xia, W.X.; Wang, W.H.; Wang, J.Q.; Huo, J.T. Giant refrigerant capacity in Gd-based amorphous/nanocrystalline composite fibers. *Mater. Today Phys.* **2021**, *21*, 100528. [[CrossRef](#)]
- Yin, H.B.; Law, J.Y.; Huang, Y.Y.; Franco, V.; Shen, H.X.; Jiang, S.D.; Bao, Y.; Sun, J.F. Design of Fe-containing GdTbCoAl high-entropy-metallic-glass composite microwires with tunable Curie temperatures and enhanced cooling efficiency. *Mater. Des.* **2021**, *206*, 109824. [[CrossRef](#)]
- Lai, J.W.; Zheng, Z.G.; Zhong, X.C.; Franco, V.; Montemayor, R.; Liu, Z.W.; Zeng, D.C. Table-like magnetocaloric effect of $\text{Fe}_{88-x}\text{Nd}_x\text{Cr}_8\text{B}_4$ composite materials. *J. Magn. Magn. Mater.* **2015**, *390*, 87–90. [[CrossRef](#)]
- Yuan, F.; Li, Q.; Shen, B.L. The effect of Fe/Al ratio on the thermal stability and magnetocaloric effect of $\text{Gd}_{55}\text{Fe}_x\text{Al}_{45-x}$ ($x = 15\text{--}35$) glassy ribbons. *J. Appl. Phys.* **2012**, *111*, 07A937. [[CrossRef](#)]
- Wu, C.; Ding, D.; Xia, L.; Chan, K.C. Achieving tailorable magneto-caloric effect in the Gd-Co binary amorphous alloys. *AIP Adv.* **2016**, *6*, 035302. [[CrossRef](#)]
- Du, J.; Zheng, Q.; Li, Y.B.; Zhang, Q.; Li, D.; Zhang, Z.D. Large magnetocaloric effect and enhanced magnetic refrigeration in ternary Gd-based bulk metallic glasses. *J. Appl. Phys.* **2008**, *103*, 023918. [[CrossRef](#)]
- Tang, B.Z.; Xie, H.X.; Li, D.M.; Xia, L.; Yu, P. Microstructure and its effect on magnetic and magnetocaloric properties of the $\text{Co}_{50}\text{Gd}_{50-x}\text{Fe}_x$ glassy ribbons. *J. Non-Cryst. Solids* **2020**, *533*, 119935. [[CrossRef](#)]
- Zhong, X.C.; Tian, H.C.; Wang, S.S.; Liu, Z.W.; Zheng, Z.G.; Zeng, D.C. Thermal, magnetic and magnetocaloric properties of $\text{Fe}_{80-x}\text{M}_x\text{B}_{10}\text{Zr}_9\text{Cu}_1$ ($M = \text{Ni, Ta}$; $x = 0, 3, 5$) amorphous alloys. *J. Alloys Compd.* **2015**, *633*, 188–193. [[CrossRef](#)]
- Yu, P.; Zhang, J.Z.; Xia, L. Effect of boron on the magneto-caloric effect in $\text{Fe}_{91-x}\text{Zr}_9\text{B}_x$ ($x = 3, 4, 5$) amorphous alloys. *J. Mater. Sci.* **2017**, *52*, 13948–13955. [[CrossRef](#)]
- Wang, X.; Wang, Q.; Tang, B.Z.; Ding, D.; Li, C.; Xia, L. Magnetic and magneto-caloric properties of the amorphous $\text{Fe}_{92-x}\text{Zr}_8\text{B}_x$ ribbons. *Materials* **2020**, *13*, 5334. [[CrossRef](#)]
- Guo, D.Q.; Yuan, Y.D.; Chan, K.C. The effect of different minor additions on the magneto-caloric effect of FeZrB metallic ribbons near room temperature. *J. Magn. Magn. Mater.* **2018**, *446*, 12–17. [[CrossRef](#)]
- Yu, P.; Zhang, J.Z.; Xia, L. $\text{Fe}_{87}\text{Zr}_7\text{B}_4\text{Co}_2$ amorphous alloy with excellent magneto-caloric effect near room temperature. *Intermetallics* **2018**, *95*, 85–88. [[CrossRef](#)]

19. Gan, L.H.; Ma, L.Y.; Tang, B.Z.; Ding, D.; Xia, L. Effect of Co substitution on the glass forming ability and magnetocaloric effect of $\text{Fe}_{88}\text{Zr}_8\text{B}_4$ amorphous alloys. *Sci. China-Phys. Mech. Astron.* **2017**, *60*, 076121. [[CrossRef](#)]
20. Wang, C.H.; Wang, Q.; Tang, B.Z.; Zhou, X.; Ding, D.; Xia, L. Achieve good magneto-caloric response near the ambient temperature in a $\text{Fe}_{86}\text{La}_7\text{B}_5\text{Ce}_2$ amorphous ribbon. *J. Magn. Magn. Mater.* **2022**, *547*, 168954. [[CrossRef](#)]
21. Wang, Q.; Pan, L.L.; Tang, B.Z.; Ding, D.; Xia, L. Outstanding magnetocaloric properties at ambient temperature of a $\text{Fe}_{88}\text{La}_4\text{Ce}_3\text{B}_5$ amorphous alloy. *J. Non-Cryst. Solids* **2022**, *580*, 121394. [[CrossRef](#)]
22. Wang, Q.; Ding, D.; Tang, B.Z.; Yu, P.; Yao, J.L.; Xia, L. Formation and magnetocaloric properties of the amorphous $\text{Fe}_{88}\text{La}_{7-x}\text{Ce}_x\text{B}_5$ ($x = 0, 1, 3, 5, 7$) ribbons. **2022**, unpublished.
23. Ogiso, K. X-ray Diffraction Instrument. U.S. Patent No. 3868506A, 25 February 1975.
24. Ernesto, F. Differential scanning calorimetry. *Methods Mol. Biol.* **1995**, *40*, 191–218.
25. *Physical Property Measurement System User's Manual*; Quantum Design: San Diego, CA, USA, 2010.
26. Turnbull, D. Under what conditions can a glass be formed? *Contemp. Phys.* **1969**, *10*, 473–488. [[CrossRef](#)]
27. Lu, Z.P.; Liu, C.T. A new glass-forming ability criterion for bulk metallic glasses. *Acta Mater.* **2002**, *50*, 3501–3512. [[CrossRef](#)]
28. Inoue, A. Stabilization of metallic supercooled liquid and bulk amorphous alloys. *Acta Mater.* **2000**, *45*, 279–306. [[CrossRef](#)]
29. Liu, D.; Zhao, T.Y.; Shen, B.G.; Li, B.H.; Zhang, M.; Zuo, S.L.; Liu, J.; Jiang, S.D.; Hu, F.X.; Sun, J.R. Microstructures and magnetic properties of Co-substituted Ce-Fe-B amorphous alloys. *J. Alloys Compd.* **2019**, *820*, 153098. [[CrossRef](#)]
30. Song, M.N.; Huang, L.W.; Tang, B.Z.; Ding, D.; Wang, X.; Xia, L. Enhanced Curie temperature and magnetic entropy change of $\text{Gd}_{63}\text{Ni}_{37}$ amorphous alloy by Co substitution. *Intermetallics* **2019**, *115*, 106614. [[CrossRef](#)]
31. Franco, V.; Blázquez, J.S.; Conde, A. Field dependence of the magnetocaloric effect in materials with a second order phase transition: A master curve for the magnetic entropy change. *Appl. Phys. Lett.* **2006**, *88*, 222512. [[CrossRef](#)]
32. Li, Z.B.; Zhang, L.L.; Zhang, X.F.; Li, Y.F.; Zhao, Q.; Zhao, T.Y.; Shen, B.G. Tunable Curie temperature around room temperature and magnetocaloric effect in ternary Ce–Fe–B amorphous ribbons. *J. Phys. D Appl. Phys.* **2017**, *50*, 015002. [[CrossRef](#)]
33. Wu, Y.B.; Wang, Q.; Tang, B.Z.; Pan, L.L.; Ding, D.; Xia, L. Outstanding glass formability and magneto-caloric effect of a $\text{Fe}_{85}\text{Co}_3\text{Zr}_5\text{B}_4\text{Nb}_3$ metallic glass. *J. Non-Cryst. Solids* **2021**, *566*, 120885. [[CrossRef](#)]
34. Chen, L.S.; Zhang, J.Z.; Wen, L.; Yu, P.; Xia, L. Outstanding magnetocaloric effect of $\text{Fe}_{88-x}\text{Zr}_8\text{B}_4\text{Sm}_x$ ($x = 0, 1, 2, 3$) amorphous alloys. *Sci. China-Phys. Mech. Astron.* **2018**, *61*, 056121. [[CrossRef](#)]
35. Wang, X.; Wang, Q.; Tang, B.Z.; Ding, D.; Li, C.; Xia, L. Effect of Mn substitution Fe on the formability and magnetic properties of amorphous $\text{Fe}_{88}\text{Zr}_8\text{B}_4$ alloy. *Metals* **2021**, *11*, 1577. [[CrossRef](#)]
36. Boutahar, A.; Lassri, H.; Hlil, E.K.; Fruchart, D. Critical behavior and its correlation with magnetocaloric effect in amorphous $\text{Fe}_{80-x}\text{V}_x\text{B}_{12}\text{Si}_8$ ($x = 8, 10$ and 13.7) alloys. *J. Magn. Magn. Mater.* **2016**, *398*, 26–31. [[CrossRef](#)]
37. Law, J.Y.; Ramanujan, R.V.; Franco, V. Tunable Curie temperatures in Gd alloyed Fe–B–Cr magnetocaloric materials. *J. Alloys Compd.* **2010**, *508*, 14–19. [[CrossRef](#)]